POLITECNICO DI TORINO
Repository ISTITUZIONALE

Verification and validation of mHIT code over TMAP for hydrogen isotopes transport studies in fusion-relevant environments

Original
Verification and validation of mHIT code over TMAP for hydrogen isotopes transport studies in fusion-relevant environments / Candido, L., Alberghi, C.. - In: FUSION ENGINEERING AND DESIGN. - ISSN 0920-3796. - 172:(2021), p. 112740. [10.1016/j.fusengdes.2021.112740]

Availability:
This version is available at: 11583/2911194 since: 2021-07-09T12:32:49Z

Publisher:
Elsevier

Published
DOI:10.1016/j.fusengdes.2021.112740

Terms of use:

This article is made available under terms and conditions as specified in the corresponding bibliographic description in the repository

Publisher copyright
Elsevier postprint/Author's Accepted Manuscript

© 2021. This manuscript version is made available under the CC-BY-NC-ND 4.0 license
http://creativecommons.org/licenses/by-nc-nd/4.0/.The final authenticated version is available online at:
http://dx.doi.org/10.1016/j.fusengdes.2021.112740

(Article begins on next page)

11 October 2026

Verification and Validation of mHIT Code Over TMAP for Hydrogen Isotopes Transport Studies in Fusion-relevant Environments

Luigi Candido[a,*], Ciro Alberghi[a]

[a] *ESSENTIAL Group, Politecnico di Torino - Corso Duca degli Abruzzi, 24, 10129, Torino, Italy*

Abstract

The accurate prediction of tritium inventory and permeation fluxes in the breeding blanket of a D-T fusion reactor is a key aspect for future thermonuclear power plants licensing. Tritium permeation into structural materials could give rise to potential issues concerning the fuel self-sufficiency and can be lost into the environment with resulting radiological risks for the population. In the frame of hydrogen isotopes transport modelling, the Tritium Migration Analysis Program (TMAP) code is considered a referred code for the safety design of nuclear fusion power plants. It is mainly applied to Plasma Facing Components (PFCs), which are subjected to intense particles implantation and surface heat fluxes.

Due to some code limitations and to the need of having a more easy-to-use computer code in a multiphysics framework, in the last years the commercial software COMSOL Multiphysics has been used to assess tritium transport studies as an application to ITER, DEMO and CFETR fusion reactors, but it was never validated against TMAP. Within this paper, a COMSOL-based code named mHIT (multi-trapping Hydrogen Isotopes Transport code) is presented. A set of verification and validation (V&V) problems were addressed, with the aim of substantiating the capabilities of the code in common fusion-relevant experimental set-ups and to include different physics according to the level of detail needed for a given application.

Keywords: COMSOL, TMAP, Hydrogen Isotopes, Transport

1. Introduction

In fusion thermonuclear reactors, the development of tritium transport models has become a key aspect for the correct estimates of tritium retention and permeation through the steels and the coolant towards the external environment [1]. Within this frame, the Tritium Migration Analysis Program (TMAP) code has been widely used for the description of deuterium (D) and/or tritium (T) implantation, diffusion and trapping since the 1980s in numerous applications, becoming a referred code for the safety design of nuclear fusion power plants. The applications regard experiments in support to fusion safety, predictions for the International Thermonuclear Experimental Reactor (ITER), and, in general, evaluations concerning tritium production technologies [2, 3]. Still today, TMAP7 is widely used [4, 5, 6] in estimating the tritium inventory in Plasma Facing Components (PFCs), which are subjected to intense rates of plasma ionic species implantation as well as severe surface heat fluxes up to 10 MW m^{-2} [7].

TMAP7 is a FORTRAN-based hydrogen isotopes transport code which calculates the time-dependent response of up to 10 gaseous diffusing species in solid structures, managing up to 50 separate diffusion segments for a total of 1000 nodes. Thermal calculations are also supported, including conduction, convection and heat generation. The different domains are allowed to interact from the point of view of both thermal response and chemical reactions. One of the most important features of TMAP7 is the possibility to include up to 3 trap types, although recent updates of the code [8] extend the trap site model to treat arbitrary numbers of trappings.

However, one of the drawbacks of TMAP is the limitation to 1D models, which makes the tool not suitable for complex geometries such as the ones encountered in the breeding blankets. Moreover, the multiphysics is strongly limited to heat transfer, flows between the different domains, and chemical reactions within them. In a liquid metal breeding blanket, such as the Water-Cooled Lithium-Lead (WCLL) concept, more complex phenomena influence the lithium-lead velocity profile, e.g. the magnetohydrodynamics (MHD) effect [9], and as a consequence the transport process of hydrogen isotopes is strongly modified. These phenomena need to be taken into account for a correct description of the transport process [10].

This work is focused on the verification and validation of the new mHIT code, developed with COMSOL Multiphysics, over TMAP; mHIT is an upgrade of the previous HIT code developed for 1D and 2D applications [11]. It has the capability to treat multiple traps and includes an interface for the implementation of chemical reactions between

*Corresponding author
Email address: luigi.candido@polito.it (Luigi Candido)

the different species. In order to be used in fusion-relevant applications, such as for example [12, 13, 14, 15, 16], a comprehensive benchmark activity is mandatory. In general, one of this code is its capability to adopt Equation Based (EB) modelling, which allows the implementation of user-defined equations and then arbitrarily increase the level of detail of the mathematical treatment. In order to catch the main TMAP features, the benchmark of mHIT was conducted according to [3] on 11 problems, selected among the most significant cases involving hydrogen isotopes transport. The boundary conditions are the same as those in [3] and then not reported here.

The structure of the paper is hereafter described. Section 2 shows the verification cases on analytical results. The following cases were analysed:

1. Diffusion from a depleting source;
2. Diffusion in a semi-infinite slab with constant-source Boundary;
3. Diffusion in a partially preloaded semi-infinite slab;
4. Effective diffusivity trap;
5. Strong trap;
6. Multiple trap;
7. Diffusion with composite material layers.

In Section 3 the validation of experiments are reported. In particular, the benchmark was conducted on:

1. Ion implantation experiment;
2. Diffusion experiment in beryllium;
3. Test cell release experiment;
4. Thermal desorption spectroscopy on tungsten.

Finally, Section 4 is dedicated to the discussion of the results and conclusions.

2. Verification cases

2.1. Diffusion from a depleting source

This model describes the time-dependent diffusion from a domain containing gaseous tritium through a silicon carbide (SiC) layer of thickness $\delta = 33$ μm. The temperature is $T = 2373$ K. It is assumed that the surface in contact with the gas is in equilibrium with the gas itself. From a mathematical viewpoint, the problem can be written as:

$$\frac{\partial c(x,t)}{\partial t} - D\frac{\partial^2 c(x,t)}{\partial x^2} = 0 \tag{1}$$

where $c(x,t)$ [mol m^{-3}] is the tritium concentration in the silicon carbide layer and $D = 2.62 \cdot 10^{-11}$ m^2 s^{-1} is the diffusion coefficient. At $t > 0$ tritium is allowed to diffuse through the slab, initially kept at zero concentration.

The solution is given in terms of fractional release $FR = c/c_0$ as reported in Equation 2. This solution was adapted from the one by *Carslaw and Jaeger* for the analogous heat transfer problem [17].

$$FR = 1 - \sum_{i=1}^{\infty} \frac{2\left[(\alpha_i/\delta)^2 + L^2\right] e^{[-D(\alpha_i/\delta)^2 t]} \sin(x\alpha_i/\delta)}{\alpha_i/\delta\{\delta[(\alpha_i/\delta)^2 + L^2] + L\}} \tag{2}$$

where where L [m^{-1}] is the reciprocal of the characteristic length of the problem, $c_0 = Sp/N_A$ (Henry's law) is the boundary concentration, $S = 3.05 \cdot 10^{19}$ J^{-1} is the solubility, $p = 1 \cdot 10^6$ Pa is the tritium pressure, and α_i [-] are the $i-$th roots of the transcendetal equation:

$$\alpha \tan \alpha - L\delta = 0 \tag{3}$$

It should be observed that Equation 3 comes from the solution technique based on variables separation, where the α_i coefficients represent the eigenvalues associated to the ordinary differential equations obtained. More details on the derivation of Equation 2 and Equation 3 can be found in Chapter 3.13 of Ref. [17]. In the calculations, the first 10 roots of Equation 3 are considered. The characteristic length is expressed as $L = S \cdot T \cdot A \cdot k_B/V$, where $A = 2.16 \cdot 10^{-6}$ m^2 and $V = 5.20 \cdot 10^{-11}$ m^3 are the surface and the volume of the domain, respectively, and k_B [J K^{-1}] is the Boltzmann constant. In Figure 1, the results of the comparison between mHIT, TMAP and the analytical solution expressed by Equation 2 are displayed. TMAP results are plotted up to 45 s according to [2].

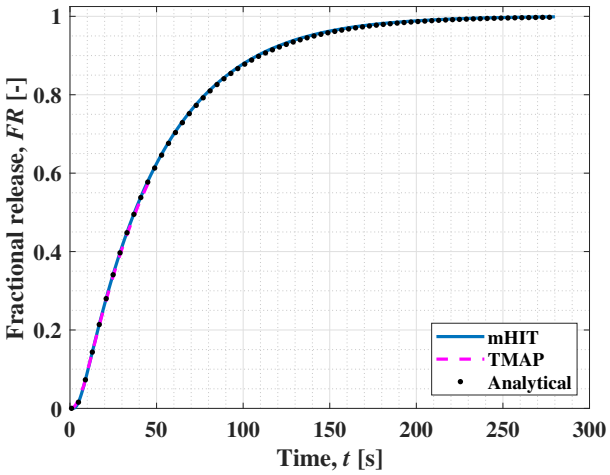

Figure 1: Time-dependent fractional release for depleting source.

It should be observed that another solution is proposed by *Evans and Morgan* [18]:

$$FR = 1 - \sum_{i=1}^{\infty} \frac{2L \sec \alpha_i e^{-\alpha_i^2 Dt/\delta^2}}{L(L+1) + \alpha_i^2} \tag{4}$$

In this case, $L = \delta A/(V\phi)$, where $\phi = 1$ expresses the ratio between the source concentration and the layer con-

centration (i.e., the concentration at the interface with the source). The α_i coefficients are the roots of:

$$\alpha \tan \alpha - L = 0 \tag{5}$$

The goodness of the benchmark was performed by evaluating the integral error, defined as:

$$\varepsilon_{num}^{an} = \left| \frac{sol_{num}}{sol_{an}} - 1 \right| \tag{6}$$

Here, $sol_{num} = \int_0^{t_{end}} f_{num}(t)\,\mathrm{d}t$ is the integral of the numerical solution, where $f_{num}(t)$ is the fractional release evaluate by means of mHIT or TMAP; on the other hand, $sol_{an} = \int_0^{t_{end}} f_{an}(t)\,\mathrm{d}t$ is the integral of the analytical solution, where $f_{an}(t)$ is the fractional release evaluated with Equation 2 or Equation 4. In other words, a comparison between the areas underneath the different curves is performed. In Table 1, the error evaluation for the fractional release was conducted up to 45 s considering the analytical solutions given by Equation 2 (labelled as CJ) and Equation 4 (labelled as EM). The mHIT model is able to guarantee the lowest error for both the analytical solutions.

Table 1: Error evaluation for depleting source.

Error type	Description	Value [%]
ε_{mHIT}^{CJ}	mHIT over CJ	0.122
ε_{mHIT}^{EM}	mHIT over EM	0.243
ε_{tmap}^{CJ}	TMAP over CJ	0.827
ε_{tmap}^{EM}	TMAP over EM	0.708

2.2. Diffusion in a semi-infinite slab with constant-source Boundary

A semi-infinite slab made of silicon carbide is kept at zero concentration for $t \leq 0$, whereas diffusion, characterised by $D = 1$ m^2 s^{-1}, is allowed for $t > 0$. The free surface is kept at constant concentration $c_0 = 1$ at m^{-3}. The mathematical equation governing the problem is the same as Equation 1. A slab of length $l = 200$ m was assumed to simulate the semi-infinite domain. The solution of this problem is given by *Carslaw and Jaeger* [17]:

$$c(x,t) = c_0 \operatorname{erfc}\left(\frac{x}{2\sqrt{Dt}}\right) \tag{7}$$

The results are reported in Figure 2. The integral error is evaluated by means of Equation 6, for which a comparison between the areas under the different curves is performed. The error reads 0.149% for mHIT and 0.0638% for TMAP. In this case, TMAP performs better than mHIT, although mHIT error is below 0.15%.

2.3. Diffusion in a partially preloaded semi-infinite slab

This problem models a semi-infinite slab in which the first $d_0 = 10$ m are preloaded with tritium at a constant concentration $c_0 = 1$ at m^{-3}. The diffusion coefficient is assumed to be $D = 1$ m^2 s^{-1}. The solution is again given by *Carslaw and Jaeger* [17]:

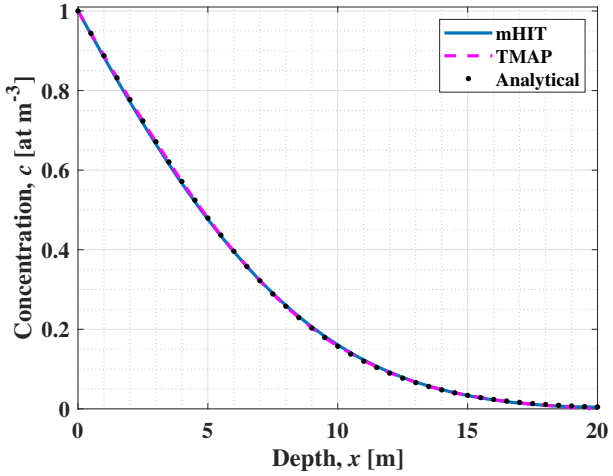

Figure 2: Concentration profile in a semi-infinite slab after 25 s.

$$c = \frac{c_0}{2}\left[2\operatorname{erf}\frac{x}{2\sqrt{Dt}} - \operatorname{erf}\frac{x-d_0}{2\sqrt{Dt}} - \operatorname{erf}\frac{x+d_0}{2\sqrt{Dt}}\right] \tag{8}$$

The results are shown in Figure 3 for the concentration history evaluated at $x = 12$ m, i.e. slightly after the preloaded domain. The error was calculated assuming a time step of 5 s [3]. The integral errors are 0.0281% and 0.0964% for mHIT and TMAP, respectively.

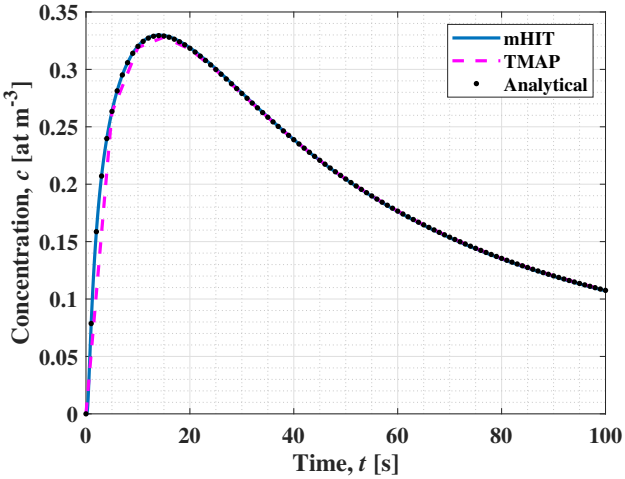

Figure 3: Concentration history at $x = 12$ m.

2.4. Effective diffusivity trap

The problems exposed in Chapter 2.1-2.3 were based on the assumption that no traps were present in the slab. To take into account the trapping phenomenon, hydrogen isotopes populations are split in mobile particles, identified by their concentration c_m, and trapped particles, identified

by their concentration c_t. In isothermal conditions, if n trapping sites are present, the basic equations governing the movement of these species are:

$$\frac{\partial c_m(x,t)}{\partial t} - D\frac{\partial^2 c_m(x,t)}{\partial x^2} = S_m - \sum_{i=1}^{n}\frac{\partial c_t^i(x,t)}{\partial t} \quad (9)$$

$$\frac{\partial c_t^i(x,t)}{\partial t} = \nu_t f_t^i c_m - \nu_r^i c_t^i \quad (10)$$

where S_m [mol m^{-3} s^{-1}] represents an external source of mobile particles, ν_t [s^{-1}] is the trapping rate coefficient, f_t^i [-] is the probability of landing in a trap site and ν_r^i [s^{-1}] is the release rate coefficient for exiting out of the trap site. In particular, $\nu_t = D/\lambda^2$, where λ [m] is the jump distance or lactice constant expressing the distance between two solute sites or between a solute and a trap site, $f_t^i = (n_t^i - c_t^i N_A)/N$, where n_t^i [at m^{-3}] is the trap density, $(n_t^i - c_t^i N_A)$ [at m^{-3}] is the number of empty sites, N [at m^{-3}] is the density of interstitial sites and $\nu_r^i = \nu_0 \exp(-E_t^i/k_B T)$, where ν_0 [s^{-1}] is the Debye frequency, E_t^i [eV] is the trap binding energy of the $i-$th trap and k_B [eV K^{-1}] is the Boltzmann constant. According to [3], it is possible to define, for each trap, a trapping parameter as:

$$\zeta_i = \frac{\lambda^2 N}{D_0 n_t^i}\nu_0 \exp\left(\frac{E_{diff} - E_t^i}{k_B T}\right) + \frac{c_m N_A}{n_t^i} \quad (11)$$

where D_0 [m^2 s^{-1}] is the pre-exponential factory in the Arrhenius-type equation for diffusivity and E_{diff} [eV] is the activation energy for diffusion. According to the value assumed by ζ_i, different trapping regimes can be identified. The case with $\zeta >> c_m N_A/n_t^i$ represents an *effective diffusivity regime* or *weak trap regime*. According to this regime, the transient permeation flux is almost equal to the no trapping case, with the exception that the diffusivity is replaced by an *effective diffusivity*:

$$D_{eff} = \frac{D_0}{1 + \sum_{i=1}^{n}\zeta_i^{-1}} \quad (12)$$

From Equation 12, it is clear that a high value of this parameter makes the effective diffusivity more similar to the diffusivity in case of no traps, i.e. $\lim_{\zeta\to\infty} D_{eff} = D$. In a weak trap regime, the breakthrough time can be defined as the intersection of the steepest tangent of the permeation transient with the time axis, i.e.:

$$\tau_{b,ed} = \frac{\delta^2}{2\pi^2 D_{eff}} \quad (13)$$

The verification case reported hereafter is a one-trap model under effective diffusivity regime. In this case, the transient permeation flux is given by:

$$J_p = \frac{c_0 D}{\delta}\left[1 + 2\sum_{m=1}^{\infty}(-1)^m \exp\left(-m^2\frac{t}{2\tau_{b,ed}}\right)\right] \quad (14)$$

In case of no trapping, the transient solution is [19]:

$$J_p = \frac{c_0 D}{\delta}\left[1 + 2\sum_{m=1}^{\infty}(-1)^m \exp\left(-m^2\frac{t}{\delta^2/\pi^2 D}\right)\right] \quad (15)$$

The input data are reported in Table 2. It should be noticed that the diffusivity was assumed to be independent of the temperature as in Ref. [3].

Table 2: Input parameters for effective diffusivity regime.

Parameter	Description	Value
λ	Lattice constant	$1 \cdot 10^{-15}$ m
c_0	Concentration	$5.25 \cdot 10^{-6}$ mol m^{-3}
D_0	Diffusivity pre-exp.	1 m^2 s^{-1}
ν_0	Debye frequency	$1 \cdot 10^{13}$ s^{-1}
n_1/N	Trapping site fraction	0.1
E_{diff}	Diffusion act. energy	0 eV
E_t^1/k_B	Trap binding energy	100 K
δ	Slab thickness	1 m
T	Temperature	1000 K

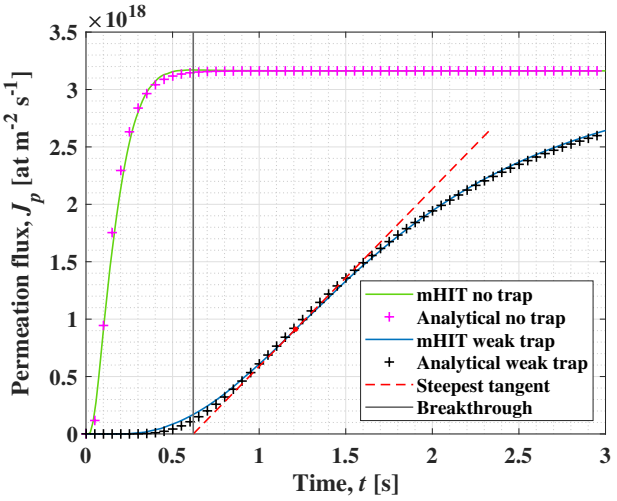

Figure 4: Permeation flux for single weak trap regime.

For sake of clarity, in Figure 4 only the results obtained with mHIT against the analytical solutions are reported. According to [3], the comparison is carried out on the breakthrough time. For TMAP, it reads 0.629 s, whereas for mHIT it is 0.620 s. The analytical value obtained with Equation 13 is 0.611 s, resulting in an error of 1.46% for mHIT and 3.02% for TMAP.

2.5. Strong trap

The *strong trap regime* applies when $\zeta << c_m N_A/n_t^i$ and no permeation occurs until all traps are filled and this happens in correspondence of the breakthrough time:

$$\tau_{b,st} = \frac{\delta^2 n_1}{2c_0^* N D} \quad (16)$$

where $c_0^* = 1 \cdot 10^{-4}$ is the surface concentration of the mobile species normalised to the lattice density and the other parameters are equal to the previous case.

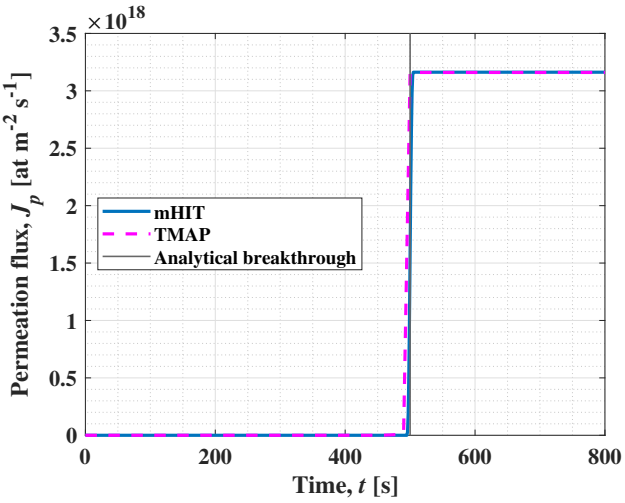

Figure 5: Permeation flux for single strong trap regime.

The comparison among the two codes is reported in Figure 5. The analytical breakthrough time is equal to 500 s. Both codes give the same numerical breakthrough, evaluated as the time needed to reach the 99% of the asymptotic value.

2.6. Multiple trap

This case was developed as an extension of the previous effective diffusivity trap, with the addition of two more trap sites. These traps are characterised by E_T^i/k_B equal to 500 K and 800 K, respectively, and a trap concentration n_t^i/N_A of 0.15 and 0.20 atom fractions. The analytical breakthrough time was evaluated by means of Equation 13 and reads 4.12 s. The effective diffusivity is $D_{eff} = 1.23{\cdot}10^{-2}$ m^2 s^{-1} which is 85% lower than the case with single trap. The results of the case with single trap and with multiple trap are reported together in Figure 6. The error comparison was performed on the breakthrough time, giving an error of 1.36% for mHIT and 4.57% for TMAP.

2.7. Diffusion with composite material layers

This model simulates a composite pyrolytic carbon (PyC) and silicon carbide (SiC) structure with a constant $c_0 = 3.05 \cdot 10^{25}$ at m^{-3} concentration on the free surface of PyC (thickness $a = 33$ μm) and a zero concentration on the free surface of SiC (thickness $l = 66$ μm). The process is assumed to be isothermal at $T = 2373$ K. According to [3], the diffusion coefficients are taken as $D_{PyC} = 1.27 \cdot 10^{-7}$ m^2 s^{-1} and $D_{SiC} = 2.62 \cdot 10^{-11}$ m^2 s^{-1}. It should be observed that this model assumes equal solubilities of PyC and SiC, that leads to equal concentrations at both sides of the interface. This is a strong assumption that is not

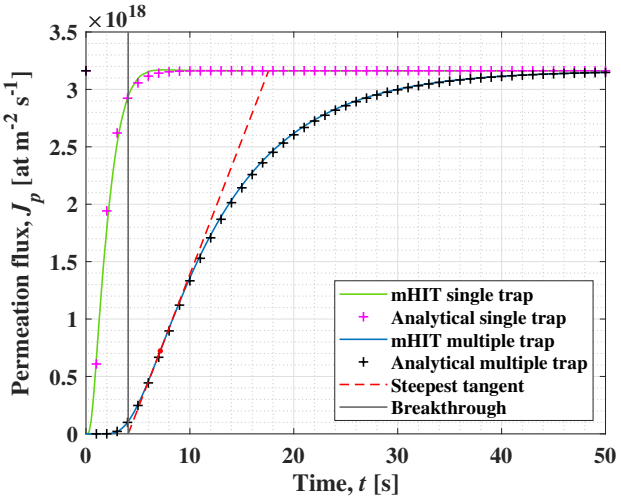

Figure 6: Permeation flux for multiple weak trap regime.

verified in fusion blankets, which present very different solubilities. Recently, COMSOL was used to deal with concentration discontinuities both in tritium transport models for the WCLL breeding blanket (see for instance Ref. [10]) and in replicating lab-scale hydrogen permeation experiments (see Ref. [20]) with a remarkable agreement between numerical and experimental values.

According to *Crank* [19], the concentration transient can be written as:

$$c = c_0 \left\{ \frac{D_{PyC}(a + l - x)}{l D_{PyC} + a D_{SiC}} - 2 \sum_{i=1}^{\infty} f_i(\lambda_i) e^{-D_{PyC} \lambda_i^2 t} \right\} \tag{17}$$

Here, $f_i(\lambda_i)$ is given by:

$$f_i(\lambda_i) = \frac{\sin(a\lambda_i) \sin(kl\lambda_i) \sin[k(l-x)\lambda_i]}{\lambda_i [a \sin^2(kl\lambda_i)] + l \sin^2(a\lambda_i)} \tag{18}$$

where $k = \sqrt{D_{PyC}/D_{SiC}}$ and λ_i [-] are the first 10 roots of the transcendental equation:

$$\tan(\lambda a) + k \tan(k\lambda l) = 0 \tag{19}$$

The solution technique adopted to obtain Equation 17 is similar to that used for Equation 2. For the same reason, the above transcendental equation occurs. In Figure 7, the concentration transient is reported for $x = 15.75$ μm, i.e. into the PyC layer of the composite material. The integral error for TMAP is 1.12%, whereas for mHIT is 0.232%.

3. Validation cases

3.1. Ion implantation experiment

The experiment performed at Idaho National Laboratory by *Anderl et al.* [21] was focused on the application

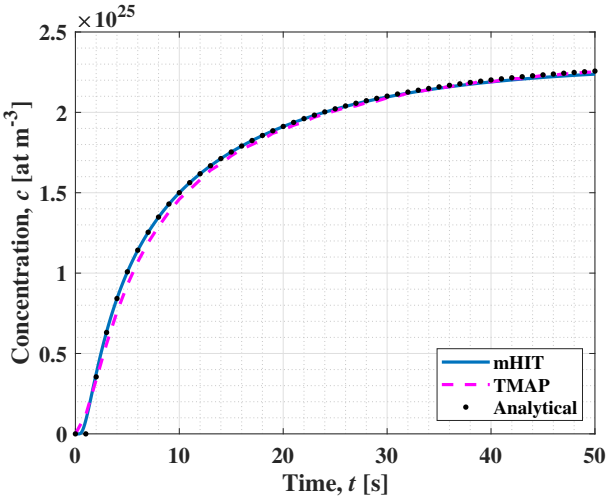

Figure 7: Concentration history 15.75 μm into the PyC layer of a PyC/SiC composite structure.

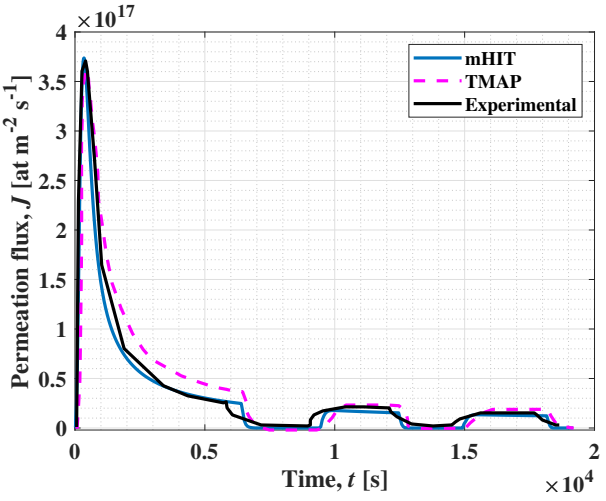

Figure 8: Plasma-driven permeation of PCA.

of a deuterium ion beam to a target characterized by a thickness $\delta = 0.5$ mm. The target was a modified AISI 316 stainless steel called Primary Candidate Alloy (PCA). The implantation depth $\delta_0 = 12$ μm was calculated in [3] with the support of TRIM code. The reflectivity coefficient, i.e. the fraction of the incident flux which is re-emitted, is assumed to be 0.25. In order to take into account the cleanup of the surface, the recombination constant of deuterium at the upstream side of the specimen was assumed to have an exponentially decreasing behaviour, i.e.:

$$k_{r,u} = 1 \cdot 10^{-27}[1 - 0.9999 \exp(-6.0 \cdot 10^{-5} t)] \qquad (20)$$

On the other hand, at the downstream side of the specimen it was assumed $k_{r,d} = 2 \cdot 10^{-31}$ m^4 at^{-1} s^{-1}. Due to vacuum conditions, the effect of pressure was neglected.

The equation describing the implantation flux as a function of time can be found in [3]. The results of the benchmark are displayed in Figure 8. It can be seen that TMAP tends to overestimate the permeation flux, with an integral error of 22.4%. mHIT solution is more precise, with an error of 5.18%.

3.2. Diffusion experiment in beryllium

This problem was taken from the work by *Macaulay-Newcombe et al.* [22], which used high-purity beryllium targets to conduct ion-implantation and thermal absorption or desorption experiments. In particular, deuterium desorption was modelled in order to reproduce Fig. 2(a) of their paper.

The sample is constituted by a polished beryllium wafer of thickness $2\delta = 0.4$ mm on which some beryllium oxide (BeO) was present; the thickness of the oxide film was measured as 18 nm. The diffusivity and solubility of deuterium in Be and BeO are reported in [3]. The sample was then exposed to 133 hPa of D_2 gas at 500 °C for 50 minutes; then, it was vacuum-cooled at 10^{-8} hPa. After that, the wafer was transferred to a thermal desorption furnace where it was heated under vacuum from ambient temperature to 800 °C at a rate of 3 °C min^{-1}. The emission rate of deuterium from the sample was measured by a residual gas analyser.

In TMAP, a two-segments model is adopted, with the two segments linked. The model was split in two parts: the former regards the charging of the sample, the latter the thermal desorption. To do this, TMAP implements a `restart` capability, by means of which it allows for alteration of equations, tables or any other input parameters. This was needed to change the diffusivity in BeO due to the phase change during thermal desorption, which results in a diffusivity 20 times higher than that of the sintered BeO. Moreover, it was needed to change the pressure between the charging phase and the thermal desorption phase. TMAP model uses its capability to perform thermal calculations through the `thermsegs` option.

In the mHIT code, as in TMAP, only half of the beryllium wafer was modelled, and this was replicated with a symmetry boundary condition. The boundary condition between BeO and Be was implemented through the partition coefficient $K = S_{BeO}/S_{Be}$. The use of the partition coefficient is equivalent to set the concentration discontinuity at the interface, preserving the continuity of the fluxes. The `restart` function of TMAP needs to re-write a substantial portion of the code, whereas in mHIT this can be easily done by adding two separate transient studies, and manually enabling the proper boundary conditions which have to be used for the specific study.

The results of the benchmark are displayed in Figure 9. The integral errors were evaluated as 5.31% and 4.32% for TMAP and mHIT, respectively.

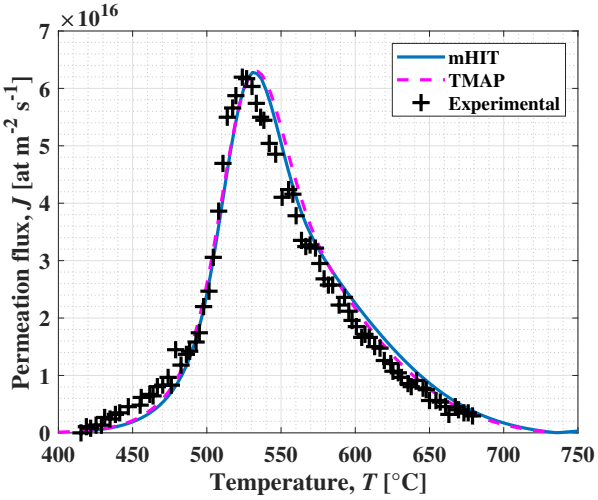

Figure 9: Thermal desorption test of beryllium.

3.3. Test cell release experiment

The following experiment was performed by *Holland and Jalbert* [23] at Los Alamos National Laboratory. It consists in a chamber of volume $V = 0.96$ m^3 internally lined with epoxy painting of thickness $\delta = 0.16$ mm. At the beginning of the experiment, air (20% r.h., $\dot{m}_{air} = 0.15$ dm^3 s^{-1}) and tritium were admitted in the chamber. The partial pressure of T_2 was 0.434 Pa, whereas the temperature was assumed equal to 303 K. The following chemical reactions between tritium and water took place:

$$T_2 + H_2O \Longrightarrow HTO + HT \quad (21)$$

$$HT + H_2O \Longrightarrow HTO + H_2 \quad (22)$$

Glycol samples were taken at fixed timed intervals from a bubbler downstream from the exposure chamber, permitting to evaluate the time-averaged concentration of HTO species with a scintillation counter. Tritium and water which were absorbed into the epoxy paint during the initial part of the test were re-emitted later.

The model in TMAP was simulated by implementing three different domains: the room from which the air is taken, the exposure chamber and the system to which the exhausts are sent. The chemical reactions were implemented for the exposure chamber only. Non-flow conditions were adopted at the interface between the paint and the chamber. Details on the chemical constants are reported in *Holland et al.* [23]. In mHIT, the Transport of Diluted Species was coupled with the Chemical Engineering module, in particular the Reaction Engineering (re) interface was used. This interface allows to implement the different chemical equations describing the problem, along with the mass balance equations for the chemical species transport. For this purpose, the Continuous-flow Stirred-Tank (CSTR) reactor model was used [24]. The results of the model developed are shown in Figure 10. The error evaluations was conducted according to Equation 6, for which it reads 0.517% for mHIT and 1.07% for TMAP.

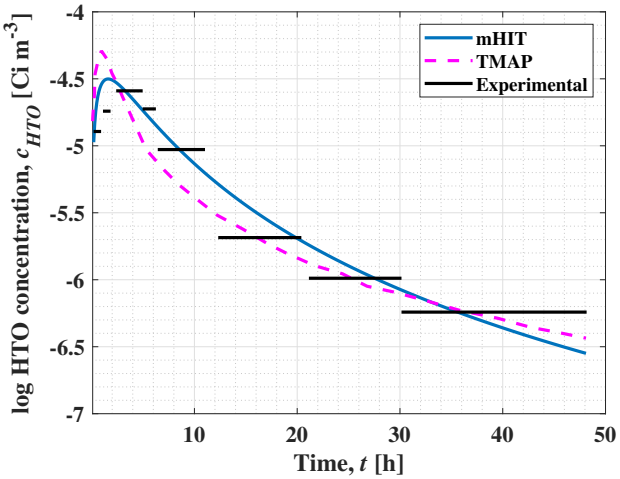

Figure 10: HTO Concentration in test cell release experiment.

3.4. Thermal desorption spectroscopy on tungsten

This experiment, performed by *Hino et al.* [25], regards the implantation of tritium ions, characterised by an energy of 5 keV and flux 10^{19} at m^{-3} s-1, into a polycristalline tungsten sheet of thickness $\delta = 0.1$ mm. The background pressure during implantation was 10^{-5} hPa and 10^{-7} hPa for the rest of the time. The Thermal Desorption Spectroscopy (TDS) was performed by heating under vacuum at 50 K min^{-1} up to 1273 K and then held at that temperature for several minutes.

The model considers three different traps. The first one was assumed to be associated with implantation and to be normally distributed with a peak at 4.6 nm and a characteristic width of 10 nm. It has to be observed that in mHIT, which uses the equation based modelling interface, it is possible to represent the space distribution of traps by simply defining a new variable corresponding to this quantity and recalling it in the general definition of the equation, in this case defined by Equation 10. The second one was a uniform trap, associated with dislocations and characterised by a trap release energy of 1.75 eV. The last one was also assumed to be uniformly distributed and to have a trapping energy of 3.1 eV. The trap concentrations were assumed equal to 0.13, 0.032 and 0.001 atomic fractions. A background drift was also considered to take into account the increasing atoms source due to the heating of the residual gas analyzer. More details on the input parameters which are not reported here can be found in [25] and [3].

The fit of the models are not exact due to several factors; one of the most important is the fact that the ion beam is not monodimensional and probably radial diffusion can occur. Secondly, uncertainties on the trap energy and density affect the results. Finally, hydrogen isotopes

exchange with the surface of the chamber may also have influenced the outcomes of the experiments. Beyond these facts, the results displayed in Figure 11 can be considered sufficient to demonstrate the utility of both the codes.

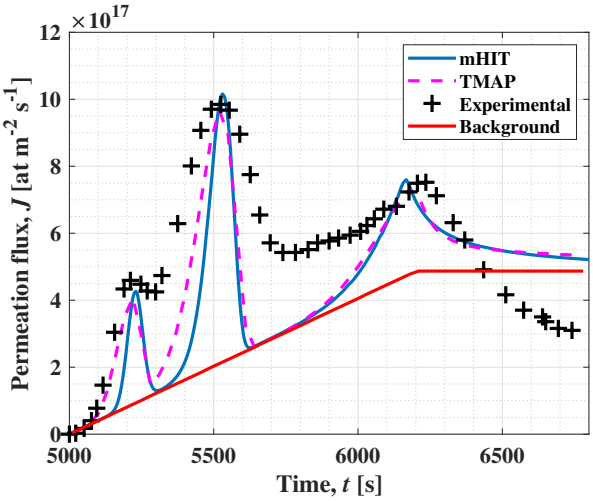

Figure 11: Results comparison for implantation and thermal desorption of tungsten.

The error was evaluated by calculating it in correspondence of the three peaks (labelled as peak 1, peak 2 and peak 3, respectively). The results of this comparison are shown in Table 3. It can be seen that for peak 1 and 3, mHIT gives better results in predicting the atomic permeation flux, whereas for peak 2 the error of TMAP is lower.

Table 3: Error comparison for TDS case.

	TMAP [%]	mHIT [%]
Peak 1	11.2	7.27
Peak 2	1.90	3.17
Peak 3	2.82	1.03

4. Discussion and conclusions

In this paper, the new mHIT code based on COMSOL Multiphysics [26] was verified and validated over some of the most relevant cases developed with TMAP. As far as verification is concerned, 7 models were solved and compared, including three trapping cases in weak trap and strong trap regimes. In general, errors below the ones of TMAP were obtained. The number of elements of the different meshes were taken equal to TMAP meshes in order to have a better estimate of the error. From the viewpoint of validation, four models were developed to reproduce some significant experiments involving hydrogen isotopes: an ion implantation experiment, a diffusion experiment in beryllium, a test cell release and a thermal desorption spectrometry experiment. Each of these models was focused to test some of TMAP capabilities, e.g. the multiphysics environment, the restart feature, the multiple traps treatment, chemical reactions and so on. These aspects were replicated with mHIT, showing that the results of mHIT are in strong agreement with TMAP, providing, in general, a lower error.

In conclusion, the work here presented showed the capability of mHIT to be used as as a tool in the frame of fusion thermonuclear reactors modelling. Its easy-to-use graphical interface allows the user to substantially reduce the time and the effort needed to write a FORTRAN-based code, adopting the same level of detail of TMAP. As a future work, mHIT will be upgraded to 3D and validated (wherever experimental tests will be available) over experimental cases needed to test other multiphysics features of the tool, for example taking into account the velocity profile of the medium in which transport of hydrogen isotopes occurs and/or the magnetohydrodynamics effect.

References

[1] I. Ricapito, A. Aiello, A. Bükki-Deme, J. Galabert, C. Moreno, Y. Poitevin, D. Radloff, A. Rueda, A. Tincani, M. Utili, Tritium technologies and transport modelling: main outcomes from the European TBM project, Fusion Engineering and Design 136 (2018) 128–134. doi:https://doi.org/10.1016/j.fusengdes.2018.01.023.

[2] G. Longhurst, D. Holland, J. L. Jones, B. J. Merrill, TMAP4 user's manual, Tech. rep., Idaho National Engineering and Environment Laboratory, USA (June 1992).

[3] G. Longhurst, TMAP7 user manual, Tech. rep., Idaho National Engineering and Environment Laboratory, USA (December 2008).

[4] G. De Temmerman, M. Baldwin, D. Anthoine, K. Heinola, A. Jan, I. Jepu, J. Likonen, C. Lungu, C. Porosnicu, R. Pitts, Efficiency of thermal outgassing for tritium retention measurement and removal in ITER, Nuclear Materials and Energy 12 (2017) 267–272, proceedings of the 22nd International Conference on Plasma Surface Interactions 2016, 22nd PSI. doi:https://doi.org/10.1016/j.nme.2016.10.016.

[5] J. Likonen, K. Heinola, A. De Backer, A. Baron-Wiechec, N. Catarino, I. Jepu, C. Ayres, P. Coad, S. Koivuranta, S. Krat, G. Matthews, M. Mayer, A. Widdowson, Investigation of deuterium trapping and release in the jet iter-like wall divertor using tds and tmap, Nuclear Materials and Energy 19 (2019) 166–178. doi:https://doi.org/10.1016/j.nme.2019.02.031.

[6] M. Shimada, C. Taylor, Improved tritium retention modeling with reaction-diffusion code TMAP and bulk depth profiling capability, Nuclear Materials and Energy 19 (2019) 273–278. doi:https://doi.org/10.1016/j.nme.2019.03.008.

[7] R. Delaporte-Mathurin, E. A. Hodille, J. Mougenot, Y. Charles, C. Grisolia, Finite element analysis of hydrogen retention in ITER plasma facing components using FESTIM, Nuclear Materials and Energy 21 (2019) 100709. doi:https://doi.org/10.1016/j.nme.2019.100709.

[8] B. J. Merrill, M. Shimada, P. W. Humrickhouse, Simulating tritium retention in tungsten with a multiple trap model in the TMAP code, Journal of Plasma and Fusion Research SERIES 10 (2013) 71–75, proceedings of the 4th Japan-China Workshop on Fusion-Related Tritium Science and Technology May 9–11, 2012, Toyama, Japan.

[9] A. Tassone, G. Caruso, F. Giannetti, A. Del Nevo, Mhd mixed convection flow in the wcll: Heat transfer analysis and cooling system optimization, Fusion Engineering and Design 146

(2019) 809–813, sI:SOFT-30. doi:https://doi.org/10.1016/j.fusengdes.2019.01.087.

[10] L. Candido, C. Alberghi, F. Moro, S. Noce, R. Testoni, M. Utili, M. Zucchetti, A novel approach to the study of magnetohydrodynamic effect on tritium transport in wcll breeding blanket of demo, Fusion Engineering and Design 167 (2021) 112334. doi:https://doi.org/10.1016/j.fusengdes.2021.112334.

[11] L. Candido, M. Cantore, E. Galli, R. Testoni, M. Utili, M. Zucchetti, An integrated hydrogen isotopes transport model for the triex-ii facility, Fusion Engineering and Design 155 (2020) 111585. doi:https://doi.org/10.1016/j.fusengdes.2020.111585.

[12] A. Ying, H. Zhang, B. Merrill, M.-Y. Ahn, S. Cho, Breeding blanket system design implications on tritium transport and permeation with high tritium ion implantation: A matlab/simulink, comsol integrated dynamic tritium transport model for hccr tbs, Fusion Engineering and Design 136 (2018) 1153–1160, special Issue: Proceedings of the 13th International Symposium on Fusion Nuclear Technology (ISFNT-13). doi:https://doi.org/10.1016/j.fusengdes.2018.04.093.

[13] A. Ying, M. Riva, M.-Y. Ahn, C. Moreno, I. Cristescu, Recent advances in tritium modeling and its implications on tritium management for outer fuel cycle, Fusion Engineering and Design 161 (2020) 111895. doi:https://doi.org/10.1016/j.fusengdes.2020.111895.

[14] H. Zhang, A. Ying, M. Abdou, Quantification of dominating factors in tritium permeation in pbli blankets, Fusion Science and Technology 68 (2) (2015) 362–367. doi:https://doi.org/10.13182/FST14-936.

[15] L. Candido, R. Testoni, M. Utili, M. Zucchetti, Tritium transport model at the minimal functional unit level for hcll and wcll breeding blankets of demo, Fusion Engineering and Design 136 (2018) 1327–1331, special Issue: Proceedings of the 13th International Symposium on Fusion Nuclear Technology (ISFNT-13). doi:https://doi.org/10.1016/j.fusengdes.2018.05.002.

[16] X. Zhao, M. Ni, B. Nie, B. Zhang, L. Chen, K. Huang, S. Liu, 3d tritium transport analysis for wccb blanket based on comsol, Fusion Engineering and Design 151 (2020) 111405. doi:https://doi.org/10.1016/j.fusengdes.2019.111405.

[17] H. S. Carslaw, J. C. Jaeger, Conduction of Heat in Solids, Second Edition, Clarendon Press, 1959.

[18] B. Evans, M. T. Morgan, Mathematical description of fission product transport in coated particles during postirradiation anneals, Tech. Rep. ORNL-4969, Oak Ridge National Laboratory, USA (June 1974).

[19] J. Crank, The mathematics of diffusion, 2nd Edition, Oxford University Press, 1975.

[20] L. Candido, M. Cantore, E. Galli, R. Testoni, M. Zucchetti, M. Utili, A. Ciampichetti, Characterization of pb-15.7li hydrogen isotopes permeation sensors and upgrade of hyper- quarch experimental device, IEEE Transactions on Plasma Science 48 (6) (2020) 1505–1511. doi:https://doi.org/10.1109/TPS.2020.2974937.

[21] R. Anderl, D. F. Holland, D. Struttmann, G. Longhurst, B. Merrill, Tritium permeation in stainless steel structures exposed to plasma ions, Proceedings of Eleventh Symposium on Fusion Engineering (SOFE) 1 (1985) 644–649.

[22] R. Macaulay-Newcombe, D. Thompson, W. Smeltzer, Deuterium diffusion, trapping and release in ion-implanted beryllium, Fusion Engineering and Design 18 (1991) 419–424. doi:https://doi.org/10.1016/0920-3796(91)90158-M.

[23] D. F. Holland, R. A. Jalbert, A model for tritium concentration following tritium release into a test cell and subsequent operation of an atmospheric cleanup system, Proceedings of Eleventh Symposium on Fusion Engineering (SOFE) 1 (1985) 638–643.

[24] Chemical Reaction Engineering Module User's Guide. COMSOL Multiphysics® v. 5.6, COMSOL AB, Stockholm, Sweden, 2020.

[25] T. Hino, K. Koyama, Y. Yamauchi, Y. Hirohata, Hydrogen retention properties of polycrystalline tungsten and helium irradiated tungsten, Fusion Engineering and Design 39-40 (1998) 227–233. doi:https://doi.org/10.1016/S0920-3796(98)00157-4.

[26] COMSOL Multiphhysics, v. 5.6, http://www.comsol.com/, Accessed: 2021-01-31.

Acknowledgements

This research did not receive any specific grant from funding agencies in the public, commercial, or not-for-profit sectors. We are grateful to Dr. Glen Longhurst from Southern Utah University for providing us TMAP7 results of the verification and validation cases reported in this article.